193 (1960).
[36]*Nuclear Data Sheets*, compiled by K. Way *et al.* (Printing and Publishing Office, National Academy of Sciences – National Research Council, Washington 25, D. C.).
[37]W. D. Hamilton, Progr. Nucl. Phys. 10, 1 (1969).
[38]T. R. Gerholm, B. G. Petterson, and Z. Grabowski, Nucl. Phys. 65, 441 (1965).
[39]P. Eerman, B. I. Deutsch, and C. J. Herrlander, Nucl. Phys. A92, 241 (1967).
[40]Nilsson single-particle states are denoted by $Nn_z\Lambda\Sigma$.
[41]B. Desplanques and N. Vinh Mau, Institut de Physique Nucléaire Report No. IPNO/TH 71-2 (unpublished).

PHYSICAL REVIEW C VOLUME 4, NUMBER 3 SEPTEMBER 1971

Quantitative Studies of Nuclear Structure Through Isobaric Analog Resonances*

S. Darmodjo, R. D. Alders, D. G. Martin, P. Dyer, S. Ali, and S. A. A. Zaidi
The University of Texas, Austin, Texas 78717
(Received 20 April 1971)

Isobaric analog resonances (IAR) observed in the elastic scattering of protons from ^{208}Pb, ^{138}Ba, ^{124}Sn, and ^{120}Sn are analyzed in the framework of the shell-model theory of reactions. Parametrization of the energy-averaged S matrix elements given by the shell-model theory is discussed, and the dependence of the spectroscopic factors upon the various optical-model parameters is exhibited. The resonance mixing phases for most of the IAR analyzed here cannot be distinguished from zero. Damping of the single-particle wave functions arising from the nonlocality of the optical potentials is consistently incorporated. The nonlocality length of 0.85 F employed in this analysis leads to an attenuation of the single-particle wave functions by about 15% inside the nucleus. Neutron spectroscopic factors obtained here compare favorably with corresponding results from the study of (d, p) and (t, d) reactions.

I. INTRODUCTION

Since the discovery of isobaric analog resonances (IAR) in heavy nuclei,[1] a large number of these resonances have been studied in various nuclei. Most frequently, they have been observed in the excitation functions of the elastically scattered protons; however, in many cases the elastic scattering data have been supplemented by measurements of the cross sections for (p, p'), (p, n), and (p, γ) reactions proceeding through IAR. Soon after the experimental identification of the observed anomalies as IAR, Robson[2] formulated a theory in the framework of the R-matrix approach[3,4] to explain the nature of these resonances. Subsequently, several different theoretical formulations of IAR have appeared in the literature.[5-15] It is generally believed that important nuclear-structure information regarding the parent analog state may be deduced from analog resonances. Thus, the elastic proton decay width of an IAR is related to the neutron spectroscopic factor of the parent analog state. Based upon the theories of IAR, several methods have been developed for extracting the neutron spectroscopic factors from the measured elastic scattering cross sections. Application of these methods yields neutron spectroscopic factors that are in good agreement with those determined from distorted-wave Born-approximation (DWBA) analysis of (d, p) reactions. It is important to study the methods for extracting the spectroscopic factors from IAR in a systematic way. In this manner, one expects to gain more insight into the nature of IAR, as well as develop a useful tool for spectroscopy. Several methods for extracting spectroscopic factors from IAR have been compared and analyzed by Harney and Weidenmüller.[16] These authors point out that the determination of the resonance mixing phase, first introduced by Robson,[2] would help clarify a number of unresolved questions regarding the external and internal mixing of the IAR. A knowledge of the resonance mixing phase, it is hoped, would also help in determining the validity of the statistical assumptions that are involved in arriving at the expressions for the energy-averaged scattering matrix elements.

In this paper we describe, in some detail, a method reported earlier and apply it to extract neutron spectroscopic factors from the measured cross sections for the elastic scattering of protons from ^{208}Pb, ^{138}Ba, ^{124}Sn, and ^{120}Sn. One of the main objectives of this study was to explore the dependence of the extracted spectroscopic factors upon the parameters of the optical potentials used to generate the energy-averaged scattering matrix elements. In Sec. II we briefly review the shell-model approach leading to the energy-averaged scattering matrix elements derived in Refs. 11, 13, and 7 and write down the expressions rele-

vant to the elastic scattering case. In addition, we calculate the proton partial width of an "ideal" IAR, whose parent analog is a pure single-neutron state. The calculation is done in the framework of the phenomenological Lane model. In Sec. III we briefly describe the technique used in obtaining some of the experimental data analyzed in this paper. Section IV contains a description of our method of analysis. The results are presented and discussed in Secs. V and VI, respectively.

II. THEORY

Reminder of the Shell-Model Approach

The analysis presented here is based upon the shell-model approach to reaction theory. Theories of IAR based on this approach have been developed by several authors. Here we follow a variation discussed by Mekjian and MacDonald[11] and in Refs. 13 and 7. The reason for this choice is a practical one. This stems from the fact that the independent-particle Hamiltonian of this shell-model treatment is very similar to the empirically known optical-model potentials for neutrons and protons. In the following we briefly recall the basic ideas of this formulation.

The nuclear Hamiltonian H is split up into an independent-particle Hamiltonian H_0 and the residual interaction V,

$$H = H_0 + V\,, \tag{2.1}$$

where

$$H_0 = \sum_{i=1}^{A} \{K_i + [\tfrac{1}{2} - t_z^{(i)}]\, v_c(i) + [\tfrac{1}{2} - t_z^{(i)}]\, v_p(i) + [\tfrac{1}{2} + t_z^{(i)}]\, v_n(i)\} \tag{2.2}$$

and

$$V = \sum_{i<k} v(i,k) - \sum_i [\tfrac{1}{2} - t_z^{(i)}]\, v_p(i) - \sum_i [\tfrac{1}{2} + t_z^{(i)}]\, v_n(i)\,. \tag{2.3}$$

Here K_i denotes the kinetic energy operator for the ith nucleon. Similarly, $v_c(i)$ denotes the average Coulomb potential for the ith nucleon. The averaged one-body potentials for protons and neutrons are denoted by $v_p(i)$ and $v_n(i)$. Finally, $v(i,k)$ is the nuclear two-body interaction and $t_z^{(i)}$ the third component of isospin of the ith nucleon. For simplicity, we imagine the target nucleus to be a doubly-closed-shell nucleus with neutron excess.

As a first step, the nuclear Hamiltonian H is diagonalized on the following set of eigenstates of H_0: (1) a proton in the proton single-particle orbit corresponding to the first vacant neutron orbit and the rest of the nucleons in the shell-model configurations corresponding to the target nucleus, and (2) the set of 2p-1h states obtained by adding a neutron in the first vacant neutron orbit and converting one of the excess neutrons into a proton. It should be observed that the independent-particle Hamiltonian H_0 is charge *dependent*; consequently, the corresponding neutron and proton orbits, referred to above, are *a priori* not identical. The correspondence pertains to the angular momentum and radial quantum numbers of the two orbits being identical. The states resulting from this diagonalization are very close to being eigenstates of analog spin[17] and also of isospin.[13] In particular, one eigenstate Φ_Σ is pushed up in energy and lies close to the energy of the IAR of the parent analog state obtained as the ground state of the target-plus-neutron system. With optimum choice of single-particle potentials the single-proton state mentioned above lies in continuum, usually occurring very far below the Coulomb barrier as an extremely sharp single-particle resonance. This difficulty may, however, be easily remedied by deepening the proton potential and including the additional potential in the residual interaction.[18] Next we imagine H diagonalized on the space of more-complicated bound eigenstates of H_0 than considered above. This gives rise, in the vicinity of IAR, to the complicated states Φ_i, also referred to as "fine-structure states" and "sea of $T_<$ states." In addition to the bound eigenstates of H_0, we consider the continuum eigenstates of H_0 involving the target nucleus and a proton in the continuum with quantum numbers characterized by μ and energy ϵ. These functions are denoted by $\psi_{\mu\epsilon}$. The radial part of the wave function of the nucleon in continuum which we denote by $F_{\mu\epsilon}$ is the regular solution of the radial Schrödinger equation. It has the asymptotic behavior

$$F_{\mu\epsilon} \sim \left(\frac{2m}{\pi\hbar^2 k r^2}\right)^{1/2} \sin(kr - \tfrac{1}{2}\pi l - \eta \ln 2kr + \delta_\mu)\,. \tag{2.4}$$

The functions $\psi_{\mu\epsilon}$ satisfy the relation

$$\langle \psi_{\mu\epsilon} | \psi_{\nu\epsilon'} \rangle = \delta_{\mu\nu}\delta(\epsilon - \epsilon')\,. \tag{2.5}$$

We define the matrix elements

$$V_{\mu\epsilon}^{(\Sigma)} = \langle \Phi_\Sigma | V | \psi_{\mu\epsilon} \rangle\,, \tag{2.6}$$

$$V^{(\Sigma i)} = \langle \Phi_\Sigma | V | \Phi_i \rangle\,, \tag{2.7}$$

$$V_{\mu\epsilon}^{(i)} = \langle \Phi_i | V | \psi_{\mu\epsilon} \rangle\,. \tag{2.8}$$

The expressions for the energy-averaged scattering matrix elements may now be obtained if one invokes the following statistical assumptions

$$\langle V_{\mu\epsilon}^{(i)} V_{\nu\epsilon'}^{(i)} \rangle_{\rm av} = \delta_{\mu\nu} \langle V_{\mu\epsilon}^{(i)} V_{\nu\epsilon'}^{(i)} \rangle_{\rm av}\,, \tag{2.9}$$

$$\langle V^{(i\Sigma)} V_{\mu\epsilon}^{(\Sigma)} \rangle_{\rm av} = 0\,. \tag{2.10}$$

Here the brackets indicate an average over the set of states $\{\Phi_i\}$. In the notation of Ref. 13 we now

write the expression for the energy-averaged S matrix elements

$$\langle S_{\lambda\mu}\rangle_{\rm av} = e^{i(\delta_\lambda+\delta_\mu)}\left\{\delta_{\mu\nu}\frac{1-Y_\lambda+2i[\Delta_{\lambda E}^{(\Sigma)}/\Gamma_{\lambda E}^{(\Sigma)}]Y_\lambda}{1+Y_\lambda+2i[\Delta_{\lambda E}^{(\Sigma)}/\Gamma_{\lambda E}^{(\Sigma)}]Y_\lambda} - i\frac{[\tilde\Gamma_{\lambda E}^{(\Sigma)}]^{1/2}[\tilde\Gamma_{\mu E}^{(\Sigma)}]^{1/2}}{E-\mathcal{E}+\frac{1}{2}iG}\right\}. \quad (2.11)$$

Here δ_λ and δ_μ are the phase shifts determined by the real potential v_p introduced in Eq. (2.2). The quantities Y_λ and $(\tilde\Gamma_{\lambda E}^{(\Sigma)})^{1/2}$ are defined as follows:

$$Y_\lambda = (\pi^2/d)\langle (V_\mu^{(i)})^2\rangle_{\rm av}, \quad (2.12)$$

$$[\tilde\Gamma_{\lambda E}^{(\Sigma)}]^{1/2} = \frac{(2\pi)^{1/2}V_{\lambda E}^{(\Sigma)}}{1+Y_\lambda+2i[\Delta_{\lambda E}^{(\Sigma)}/\Gamma_{\lambda E}^{(\Sigma)}]Y_\lambda}, \quad (2.13)$$

and

$$[\Gamma_{\lambda E}^{(\Sigma)}]^{1/2} = (2\pi)^{1/2}V_{\lambda E}^{(\Sigma)}. \quad (2.14)$$

The average distance between the fine-structure states is denoted by d, and $\Delta_{\lambda E}^{(\Sigma)}$ stands for

$$\Delta_{\lambda E}^{(\Sigma)} = {\rm P}\int\frac{[V_{\lambda E}^{(\Sigma)}]^2 d\epsilon}{E-\epsilon}. \quad (2.15)$$

The definitions of $\mathcal{E}$ and G may be found in Ref. 13. In the following they are treated as fitted parameters. The Eq. (2.13) appears to define $\tilde\Gamma_{\lambda E}^{(\Sigma)}$ in an implicit manner. Actually, the ratio $\Delta_{\lambda E}^{(\Sigma)}/\Gamma_{\lambda E}^{(\Sigma)}$ is expected to be insensitive to the structure of the state Φ_Σ; in addition, the quantity Y_λ is small compared to unity in many cases. We return to this point below. The connection between the energy-averaged scattering matrix elements [Eq. (2.11)] and those given by the conventional complex optical-model potential is established by requiring

$$e^{2i\xi_\lambda} = e^{2i\delta_\lambda}\frac{1-Y_\lambda+2i[\Delta_{\lambda E}^{(\Sigma)}/\Gamma_{\lambda E}^{(\Sigma)}]Y_\lambda}{1+Y_\lambda+2i[\Delta_{\lambda E}^{(\Sigma)}/\Gamma_{\lambda E}^{(\Sigma)}]Y_\lambda}. \quad (2.16)$$

Here ξ_λ is the complex optical-model phase shift. Thus, the complex optical model is used only to parametrize the background part of the scattering matrix elements of the shell-model approach. Equation (2.16) may be used to determine Y_λ in terms of the optical-model phase shifts. It is useful to define a resonance mixing phase Φ_λ by the relation

$$e^{-i\phi_\lambda} = 2\arg\{1+Y_\lambda+2i[\Delta_{\lambda E}^{(\Sigma)}/\Gamma_{\lambda E}^{(\Sigma)}]Y_\lambda\}. \quad (2.17)$$

Comparison with the work of Ref. 11 shows that in the present framework the resonance mixing phase is brought about entirely by the indirect coupling between the analog state Φ_λ and the fine-structure states $\{\Phi_i\}$ through the open channels $\psi_{\lambda E}$. This coupling causes a correlation between the matrix elements $V^{(i\Sigma)}$ and $V_{\mu\epsilon}^{(i)}$ leading to the expression (2.17) for the resonance mixing phase. Other contributions to the resonance mixing phase have been discussed by Mekjian and MacDonald[11] and by Harney and Weidenmüller.[16] The resonance mixing phase is also discussed in a somewhat different framework by Robson and Lane.[19] Within the framework of the Kerman and De Toledo-Piza[9] theory a specific contribution to the resonance mixing phase arising from the mixing between the analog and the antianalog state is evaluated by Auerbach *et al.*[20] for the IAR in ^{89}Y. Finally Harney[21] and Bund and Blair[14] have calculated the resonance mixing phases for a number of IAR in various nuclei and compared the results with the experimental data.

In the present framework the calculation of the resonance mixing phase can proceed using Eqs. (2.17) and (2.15). It is important in this connection to point out that we assumed that the single-particle potential v_p was chosen such that the proton single-particle state with the same angular momentum and radial quantum numbers as that of the neutron in the parent analog state is bound. With this choice, the resonance mixing phase is expected to be a small positive quantity. The optical-model potential known empirically from the systematics of binding energies, however, predicts this state to lie in continuum, where it usually occurs as a very sharp resonance far below the Coulomb barrier. If one naively performs a calculation of the resonance mixing phase using these potentials, the single-particle resonance makes a very large contribution to the integral in Eq. (2.15). The corresponding contribution to the resonance mixing phase is large and negative. In a consistent treatment, however, one should deepen the

TABLE I. Parameters of the complex Saxon-Woods potentials used for fitting the background cross sections. The form factors of the imaginary part and the spin-orbit term are derivatives of the Saxon-Woods form factors.

	v_p (MeV)	$W_{\rm D}$ (MeV)	$V_{\rm so}$ (MeV)	r_0 (F)	a (F)	r_C (F)	r_I (F)	a_I (F)	V_1 (MeV)
^{208}Pb	$66.35-0.4E_p$	10.20	5.80	1.19	0.75	1.19	1.19	0.77	0.500
^{138}Ba	$63.4-0.4E_p$	10.00	5.80	1.23	0.65	1.23	1.23	0.69	0.750
^{120}Sn	$58.25-0.5E_p$	10.00	5.80	1.235	0.65	1.235	1.235	0.77	0.866
^{124}Sn	$56.00-0.5E_p$	9.00	5.80	1.235	0.65	1.235	1.235	0.78	0.839

potential v_p until this state is bound[18] and construct the state Φ_Σ as described above. The additional potential would have to be included as a residual interaction. Alternatively, the sharp single-particle resonance may be incorporated in the shell-model calculation using techniques discussed by Weidenmüller and Dietrich.[22] In either case one would obtain a unified treatment of the analog resonance and the antianalog resonance. In particular, the continuum wave functions used to evaluate expressions like Eq. (2.17) would no longer contain single-particle resonances. One would, however, need to calculate the coupling between the analog state and the antianalog state due to virtual transitions to the continuum. In this spirit we delete the contribution of the single-particle resonance to Eq. (2.15). This is generally quite straightforward, since the resonance is very sharp and well below the Coulomb barrier.

Lane Model

The detailed microscopic model discussed above is important for clarifying the nature of IAR; however, for the analysis of experimental data it would be desirable to replace the matrix elements $V_{\mu\epsilon}^{(\Sigma)}$ of the shell-model theory by corresponding quantities of some phenomenological approach. Such a possibility is provided by the Lane model. This model was introduced by Lane[23] for explaining the charge-exchange (p, n) reaction. Several authors[2, 24, 25] have discussed IAR in terms of this model. The coupled differential equations of this model have also been solved numerically for the analysis of experimental data on analog resonances.[26-28] We use the Lane model with real potentials to calculate phenomenologically the "ideal" decay widths of the IAR and thus avoid having to perform detailed shell-model calculations for each IAR that we analyze.

The single-particle potentials v_n and v_p introduced in Eq. (2.2) uniquely define all the parameters of the Lane model, since the form factor V_1 of the charge-exchange term $(\vec{t}\cdot\vec{T})V_1$ satisfies the relationship

$$v_n - v_p = T_0 V_1 . \tag{2.18}$$

In the framework of the Lane model one can obtain approximate expressions for the scattering matrix elements,[10, 24, 29] valid in the vicinity of IAR.

$$S_{\lambda\lambda}^{(L)} = e^{2i\delta_\lambda}\left[1 - i\frac{\Gamma_{\lambda E}^{(L)}}{E - E_R + \frac{1}{2}i\Gamma_{\lambda E}^{(L)}}\right], \tag{2.19}$$

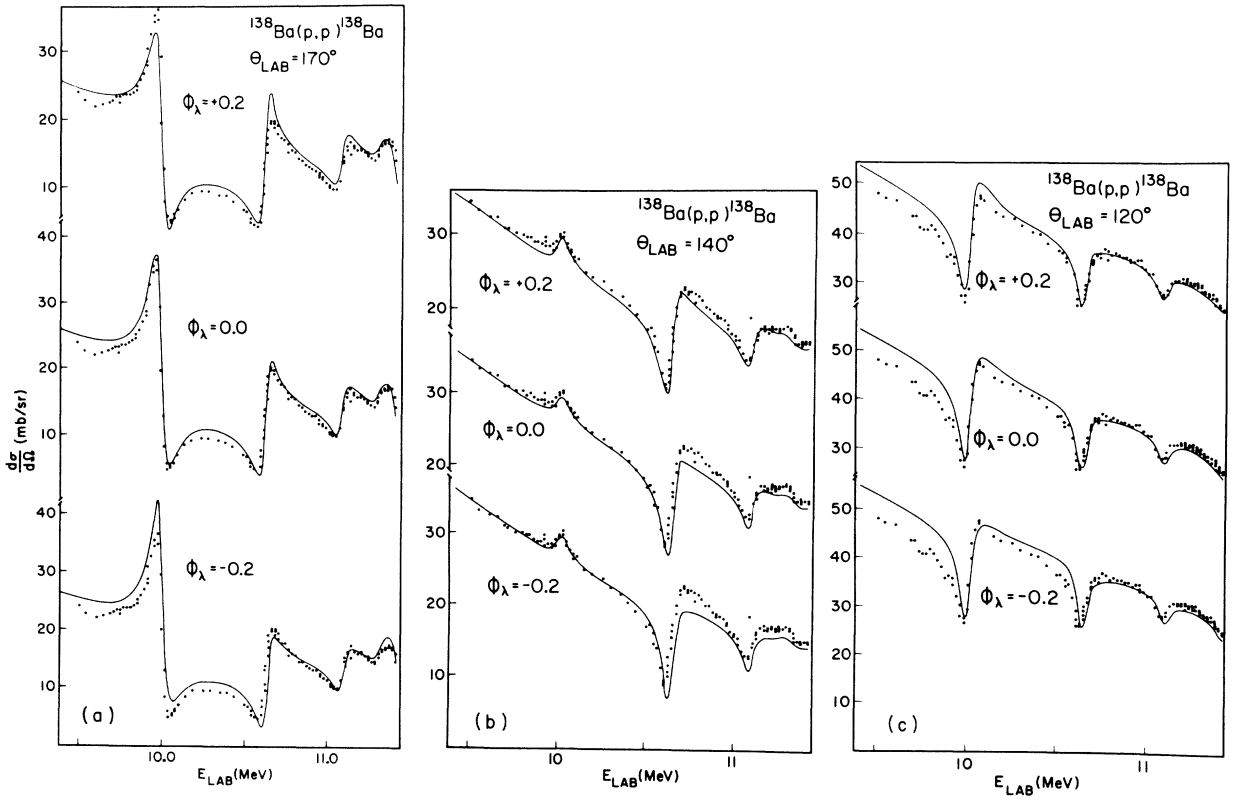

FIG. 1(a)–(c). Dependence of the calculated cross sections on the values of the resonance mixing phase ϕ_λ. All the other resonance parameters were held fixed at the optimum values obtained by setting $\phi_\lambda = 0$.

where δ_λ is the real phase shift arising from the potential scattering due to v_p and where

$$\Gamma_{\lambda E}^{(L)} = \frac{2\pi}{2T_0+1} \left| \langle \phi_{nA} | (v_n - v_p) | \psi_{\lambda E} \rangle \right|^2 . \quad (2.20)$$

The function ϕ_{nA} satisfies

$$(K + v_n - \tfrac{1}{2}V_1 + \Delta_C - E_{nA})\phi_{nA} = 0 , \quad (2.21)$$

where K is the kinetic energy operator, E_{nA} is the energy eigenvalue, and Δ_C is the Coulomb energy shift. Finally, the resonance energy E_R is given by

$$E_R = E_{nA} + \Delta_{nA}^{(L)} , \quad (2.22)$$

where

$$\Delta_{nA}^{(L)} = \frac{1}{2\pi} P' \int \frac{\Gamma_{\lambda\epsilon}^{(L)} d\epsilon}{E - \epsilon} . \quad (2.23)$$

The prime indicates that the contributions to this integral arising from the proton single-particle resonance at low energies are to be deleted. This is similar to the corresponding situation discussed in the case of the shell-model approach. The role of this proton single-particle resonance has been discussed in work of Zaidi and Coker.[30]

Expressions (2.19) and (2.20) may be compared with Eqs. (2.11) and (2.13), respectively, if one sets $Y_\lambda = 0$. The comparison suggests a unique relationship between the decay-width amplitudes of the two models. A derivation of this relationship including the possibility that the parent analog state is not a pure single-particle state is given in Ref. 16. One obtains

$$V_{\lambda\epsilon}^{(\Sigma)} = (2T_0+1)^{-1/2} S_n^{1/2} \langle \phi_{nA} | (v_n - v_p) | \psi_{\lambda\epsilon} \rangle . \quad (2.24)$$

The analysis presented in this paper employs the expressions (2.11)–(2.16) of the shell-model approach in conjunction with Eq. (2.24) to replace the decay-width amplitudes of the microscopic theory with the corresponding quantities of the Lane model. The complex optical model is used only to parametrize the background scattering.

Finally we point out that the expression (2.20) may be identically transformed into the following:

$$\Gamma_{\lambda E}^{(L)} = \frac{8\pi T_0^2}{(2T_0+1)(2T_0-1)^2} \langle \phi_{nA} | (E_p - E_{nA} + \Delta_c - v_c) | \psi_{\lambda E} \rangle^2 . \quad (2.25)$$

In deriving this result, Eq. (2.21) and the radial Schrödinger equation for the function $\psi_{\lambda E}$ have been used, and a partial integration has been performed. This result is interesting, since it does not involve the form factor of the charge-exchange term V_1 explicitly. Expressions similar to Eq. (2.25) have been used by Harney and Weidenmüller[16] and Bledsoe and Tamura.[31] Recently Clarkson, von Brentano, and Harney[32] and Clarkson, von Brentano, and Dost[33] have also used a similar expression and discussed in detail the dependence of the extracted spectroscopic factors on the optical potentials. DeToledo-Piza and Kerman[8] and Kerman[34] derive expressions for decay widths that also involve only the Coulomb interaction. It must, however, be pointed out that those expressions in-

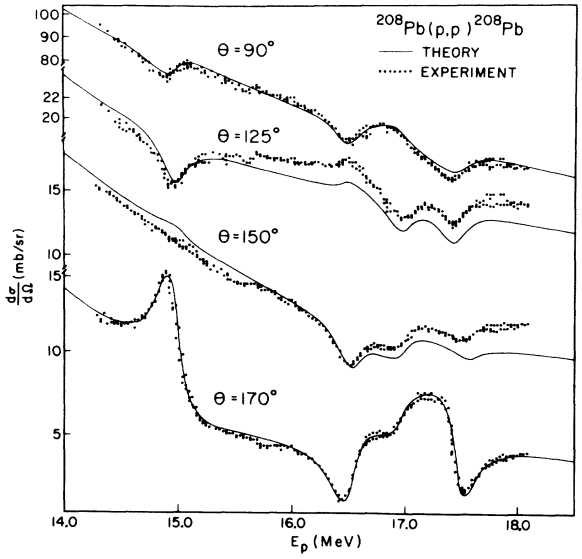

FIG. 2. Comparison of the calculated cross sections with the experimental data for ^{208}Pb$(p,p)^{208}$Pb. The parameters used in the calculation are given in Tables I and III.

TABLE II. Calculated resonance mixing phases for the IAR in ^{208}Pb, ^{138}Ba, and ^{120}Sn.

	State	Resonance energy (MeV)	$(\phi_\lambda)_{\text{Calc.}}$ (rad)
^{208}Pb	$g_{9/2}$	14.888	+0.194
	$d_{5/2}$	16.431	+0.004
	$s_{1/2}$	16.879	−0.10
	$g_{7/2}$	17.357	+0.10
	$d_{3/2}$	17.436	−0.10
^{138}Ba	$f_{7/2}$	9.932	+0.16
	$p_{3/2}$	10.555	+0.12
	$p_{1/2}$	11.008	+0.12
	$h_{9/2}$	11.234	+0.12
	$f_{5/2}$	11.345	+0.10
	$f_{5/2}$	11.633	+0.12
	$f_{5/2}$	11.826	+0.10
	$p_{1/2}$	12.092	+0.008
^{120}Sn	$d_{3/2}$	7.506	+0.19
	$s_{1/2}$	7.585	+0.19
	$d_{3/2}$	8.626	+0.21
	$d_{3/2}$	8.914	+0.18

volve continuum and bound-state functions quite different from ours.

The one-body potentials for neutrons and protons are expected to be nonlocal. One of the consequences of the nonlocality is that the single-particle wave functions of a nonlocal potential are damped inside the nuclear region compared to the wave functions of an equivalent local potential.[35] Effects of the nonlocal potentials have been discussed by several authors.[36-38] We use the following expression suggested by Perey and Buck[35] to correct the local wave functions for nonlocality effects:

$$\psi_{\lambda\epsilon}^{(\mathrm{NL})} = \left[1 - \frac{\mu\alpha^2}{2\hbar^2} v(r)\right]^{-1/2} \psi_{\lambda\epsilon} \,. \tag{2.26}$$

Here $v(r)$ is the local single-particle potential and μ is the nucleon mass. Throughout the following analysis we used $\alpha = 0.85$ F, as suggested by Perey.[39]

III. EXPERIMENTAL METHOD

Experimental data for the elastic scattering of protons from ^{208}Pb,[40] ^{124}Sn, and ^{120}Sn were obtained at the Center for Nuclear Studies using the beam from the tandem Van de Graaff accelerator. Excitation functions for the elastic scattering of protons from ^{138}Ba were measured at the Max-Planck-Institüt für Kernphysik at Heidelberg.[41] Lithium-drifted silicon detectors cooled to dry-ice temperature were used to measure the excitation functions at four backward angles simultaneously.

Self-supporting targets of lead and tin isotopes were made by evaporating the metals in high vacuum onto glass slides coated with a thin layer of a detergent. After evaporation the slides were allowed to cool. The metal film was peeled from the glass slides by floating it off on distilled water. The foils were than picked up on aluminum target frames and quickly dried by evacuating. This procedure is important for preventing the deterioration of lead foils. The thickness of the targets used in this experiment ranged between 0.2 and 0.5 mg/cm^2. Absolute cross sections were determined by measuring the counts per μC in the group of elastically scattered protons for each detector at energies well below the Coulomb barrier and forward scattering angles. Assuming that under these conditions one has pure Coulomb scattering we converted the counts per μC into mb/sr. This procedure was checked for the ^{208}Pb target by an independent determination of cross sections whereby the target foils were carefully weighed and the solid angle of the detectors was directly measured. The two methods agreed within 5%.

Pulses from the preamplifiers were fed into main linear amplifiers and biased amplifiers and finally analyzed using 1024-channel analog-to-digital converters in conjunction with the PDP-7 on-line computer.

IV. METHOD OF ANALYSIS

Excitation functions of the elastic proton scattering at all the angles and over the entire energy range for which data is available are fitted simultaneously using the computer code JULIUS.[42] This code is a modification of Perey's optical-model code PEREY. At each energy, the code calculates the elastic scattering cross section for all the an-

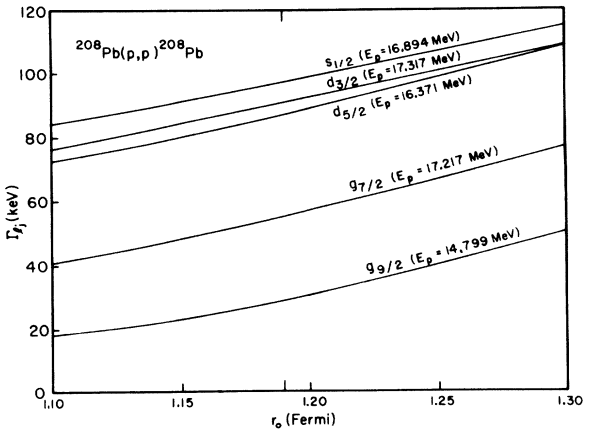

FIG. 3. Dependence of the calculated partial widths $\Gamma_{\lambda E}^{(L)}$ upon the radius parameter r_0 of the potentials. Neutron binding energy, and the magnitude of the charge-exchange term V_1, were held fixed at the values given in Tables I and III. The values given in Table III were calculated for $r_0 = 1.19$.

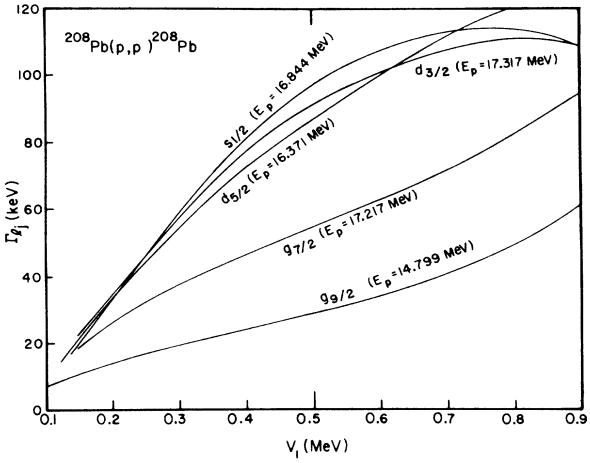

FIG. 4. Variation of the calculated partial widths $\Gamma_{\lambda E}^{(L)}$ with the magnitude of the charge-exchange term V_1. The proton wave function was calculated for each value of the proton well depths as a function of V_1. Neutron binding energy was held fixed for these calculations.

gles using the scattering matrix elements

$$S_{\lambda\lambda} = e^{2i\xi_\lambda} - ie^{2i\delta_\lambda} \frac{\Gamma_{\lambda E}^{(\mathrm{EXP})}}{E - E_R + \frac{1}{2}i\Gamma_T} . \tag{4.1}$$

The background-scattering matrix elements $e^{2i\xi_\lambda}$ are first found from the complex optical-model potential, which was chosen to have a Woods-Saxon shape with spin-orbit coupling and a surface imaginary term. Then, using the relation

$$e^{2i\xi_\lambda} = e^{2i\delta_\lambda} \frac{1 - Y_\lambda + 2i\rho_\lambda^{(\mathrm{L})} Y_\lambda}{1 + Y_\lambda + 2i\rho_\lambda^{(\mathrm{L})} Y_\lambda} , \tag{4.2}$$

where $\rho_\lambda^{(\mathrm{L})} \equiv \Delta_{nA}^{(\mathrm{L})}/\Gamma_{\lambda E}^{(\mathrm{L})}$, the values of the real quantities Y_λ and δ_λ are obtained. Treating $\Gamma_{\lambda E}^{(\mathrm{EXP})}$, E_R, and Γ_T as fitted parameters, one then calculates the cross section from Eq. (4.1). Comparing the parametrized form of the scattering matrix (4.1) to Eq. (2.11), and using Eqs. (2.13), (2.14), (2.20), and (2.24) one obtains the equation

$$\Gamma_{\lambda E}^{(\mathrm{EXP})} = \tilde{\Gamma}_\lambda^{(\Sigma)} = S_n \Gamma_{\lambda E}^{(\mathrm{L})} (1 + Y_\lambda + 2i\rho_\lambda^{(\mathrm{L})} Y_\lambda)^{-2} . \tag{4.3}$$

Thus, after using Eq. (2.20) to find the Lane width $\Gamma_{\lambda E}^{(\mathrm{L})}$, the spectroscopic factor S_n can be obtained from Eq. (4.3).

In finding the Lane width $\Gamma_{\lambda E}^{(\mathrm{L})}$ from Eq. (2.20), one needs the potentials $v_n(r)$, $v_p(r)$, and $V_1(r)$. There are four criteria that we would like to satisfy in choosing these potentials: (1) $v_n(r)$ should reproduce the binding energies of the parent analog states, (2) $v_p(r)$ should be the same as the real part of the optical-model potential which reproduces the off-resonance proton elastic scattering data, (3) V_1 should satisfy the empirical relation[23]

$$\tfrac{1}{2}T_0 V_1 = 26(N - Z)/A \tag{4.4}$$

and, (4) the relation (2.18) should be maintained. We chose to keep the same shape and radial parameters for each potential. Realizing that there is some ambiguity in determining the parameters which fit elastic scattering, we chose that set of radial parameters which best reproduced the binding energies and at the same time maintained the fit to the elastic scattering data. Then the depth for v_n (kept the same for all states in a given nucleus) was chosen as that which gave the best binding energies on the average. Having thus determined $v_n(r)$, we required that criterion (3) be satisfied in determining the depths of v_p and V_1. This meant that the v_p (chosen real) used in calculating $\Gamma_{\lambda E}^{(\mathrm{L})}$ did not exactly agree with the real part of the optical potential used to parametrize the background scattering, though they were close. In the next section we include results of the uncertainty in the Lane widths $\Gamma_{\lambda E}^{(\mathrm{L})}$ (and hence of S_n) arising from the uncertainty in the magnitude of V_1. Similarly the dependence of $\Gamma_{\lambda E}^{(\mathrm{L})}$ on the choice of parameters was also investigated.

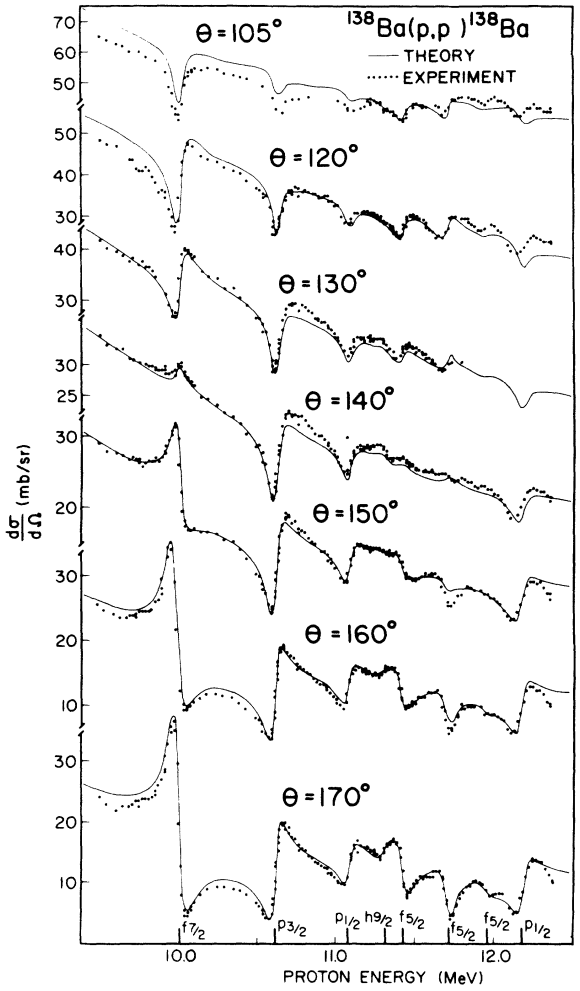

FIG. 5. Comparison of the calculated cross sections with the experimental data for ^{138}Ba$(p,p)^{138}$Ba. The parameters used in the calculation are given in Tables I and IV.

V. RESULTS

The method of analysis has been discussed in Sec. IV. We now present the results obtained. Table I shows the optical-model parameters used in the analysis of the proton elastic scattering from the target nuclei ^{208}Pb, ^{138}Ba, ^{124}Sn, and ^{120}Sn. These parameters were obtained by fitting the experimental excitation functions for each isotope simultaneously at all the angles at which data was available. The fitting procedure involved the adjustment of optical-model and resonance parameters. Initial values for the optical-model paramters for a Woods-Saxon well with spin-orbit coupling were taken from the literature. Throughout this analysis, the real part of the proton potential, the neutron potential, and the form factor of the

TABLE III. Resonance parameters, calculated partial widths, and spectroscopic factors for ^{208}Pb$(p,p)^{208}$Pb. Spectroscopic factors determined from (d,p) and (d,t) reactions are also shown for comparison.

$E_R^{(c.m.)}$ (MeV)	E_{ex} (MeV)	l	j	$\Gamma_{lj}^{(EXP)}$ (keV)	$\Gamma_{lj}^{(L)}$ (keV)	Γ_T (keV)	$(1+Y)^2$	S_{pp}	S_{dp} (Ref. 43)	S_{td} (Ref. 44)
14.888	0.000	4	$\frac{9}{2}$	21.8	28.44	260	1.29	0.98	1.04	0.93
16.431	1.543	2	$\frac{5}{2}$	40.0	85.33	275	1.82	0.86	0.99	0.86
16.879	1.991	0	$\frac{1}{2}$	41.8	95.00	300	2.06	0.90	0.94	0.86
17.357	2.469	4	$\frac{7}{2}$	29.6	53.40	275	1.52	0.84	1.05	0.90
17.436	2.548	2	$\frac{3}{2}$	39.4	88.50	275	1.93	0.86	0.97	0.83

charge-exchange term are all constrained to have the same radius parameter r_0 and diffuseness parameter a. Note that each of the potential depths has an energy dependence. These were found necessary in order to fit the slope of the cross section over the energy region of interest.

The resonance mixing phases are calculated from Eq. (2.17) and are listed in Table II for the states in ^{208}Pb, ^{138}Ba, and ^{120}Sn. Almost all of the phases have positive values of the order of 0.1–0.2. However, since the expression (2.17) for the resonance mixing phase is derived on the basis of a number of simplifying assumptions, it is not expected to be better than a rough estimate. We have actually treated the phases as fitted parameters.

In most cases, the best fit to the data was obtained with a resonance mixing phase equal to zero, although a few states (most notably the $s_{1/2}$ resonance in ^{120}Sn) did require fairly large phases in order to obtain reasonable fits. A systematic study of the effect of varying the resonance mixing phase was made, with an example of the results shown in Fig. 1. The $p_{3/2}$ resonance in ^{139}Ba is fit much better at the extreme backward angles with a zero phase, while at angles of 120–140° a positive phase of +0.2 seems to fit better. This reflects the inadequacy of the optical potentials used to generate the background scattering amplitude and shows the source of major difficulty in determining the resonance mixing phases. The effects of the phase at a particular angle depend upon the shape of the resonance at that angle. At an angle for which a resonance is high on the low-energy side and then dips below the background (e.g., the $f_{7/2}$ in Fig. 1), a shift in phase toward positive values tends to decrease the cross section all across the resonance, whereas a shift to negative values increases the cross section. The opposite behavior is observed for a resonance which dips for $E < E_R$ and then rises; a positive resonance mixing phase increases the cross section, and a negative phase decreases it. We should point out that we do not assign a nonzero phase unless we are unable to find a reasonable fit by merely varying the other resonance parameters.

^{208}Pb$(p,p)^{208}$Pb

The low-lying states in ^{209}Pb are expected to be close to being pure single-particle neutron states. We obtained by systematic search a neutron potential that reproduces the binding energies of five low-lying states in ^{209}Pb quite accurately.[29] Data

TABLE IV. Resonance parameters, calculated partial widths, and spectroscopic factors for ^{138}Ba$(p,p)^{138}$Ba. Spectroscopic factors obtained from (d,p) studies are also shown for comparison.

$E_R^{(c.m.)}$ (MeV)	E_{ex} (MeV)	l	j	$\Gamma_{lj}^{(EXP)}$ (keV)	$\Gamma_{lj}^{(L)}$ (keV)	Γ_T (keV)	$(1+Y)^2$	S_{pp}	S_{dp} (Ref. 47)
9.932	0.000	3	$\frac{7}{2}$	16.6	21.34	76	1.13	0.88	0.70
10.555	0.623	1	$\frac{3}{2}$	22.4	78.19	80	1.43	0.40	0.32
11.008	1.076	1	$\frac{1}{2}$	16.2	84.56	75	1.48	0.28	0.27
11.234	1.302	5	$\frac{9}{2}$	1.4	2.22	100	1.03	0.65	0.54
11.345	1.413	3	$\frac{5}{2}$	8.1	39.23	78	1.23	0.25	0.22
11.633	1.701	3	$\frac{5}{2}$	7.9	43.59	80	1.27	0.23	0.17
11.826	1.894	3	$(\frac{5}{2})$	2.4	47.15	100	1.29	0.06	...
12.092	2.160	1	$(\frac{1}{2})$	34.8	100.65	98	1.58	0.55	...

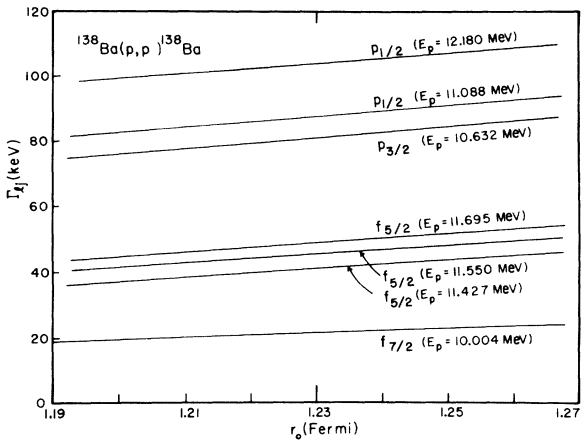

FIG. 6. Dependence of the calculated partial widths $\Gamma_{\lambda E}^{(L)}$ upon the radius parameter r_0 of the potentials. Neutron binding energy, and the magnitude of the charge-exchange term V_1, were held at the values given in Tables I and IV. The values given in Table IV were calculated for $r_0 = 1.23$.

of Ref. 40 and the calculated cross sections are shown in Fig. 2. Table III shows resonance parameters and, in particular, the spectroscopic factors. For comparison we also give the average neutron spectroscopic factors obtained by Jeans *et al.*[43] from the ^{208}Pb$(d,p)^{209}$Pb reaction below the Coulomb barrier and by Igo *et al.*[44] from the ^{208}Pb$(t,d)^{209}$Pb reaction. Our results agree quite well with those reported by Igo *et al.*[44] These authors investigated the dependence of the extracted spectroscopic factors upon the parameters of the single-particle potential used to calculate the form factor of the transferred neutron. The quoted values of the spectroscopic factors were obtained for the single-particle potential employed in this paper. Finally, we investigated the dependence of the Lane widths $\Gamma_{\lambda E}^{(L)}$ upon the radius parameter r_0 of the single-particle potentials and upon the magnitude of the charge-exchange term V_1. The results are displayed in Figs. 3 and 4. As can be seen, the width does not depend strongly on the radius parameter. Variation of the other potential parameters showed essentially the same result. However, the dependence on the charge-exchange potential V_1 is stronger, particularly for the partial waves of lower angular momentum, where varying V_1 within a range of 10% about the value prescribed by Eq. (4.4) can result in a change of the width of about 10–15%. From Eq. (2.20), it can be seen that $\Gamma_{\lambda E}^{(L)}$ depends on V_1 in two ways: (1) through the magnitude of the symmetry potential $(v_n - v_p)$ which is proportional to V_1; and (2) since as V_1 varies, Eq. (2.18) requires that the relative values of v_n and v_p change so that the overlap of the wave functions involved should also change.

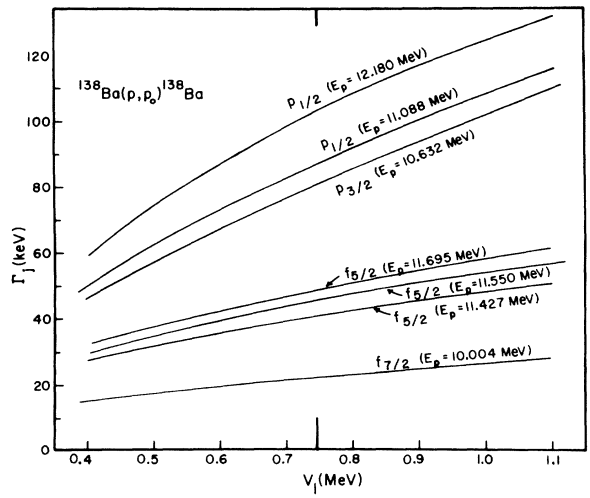

FIG. 7. Variation of the calculated partial widths $\Gamma_{\lambda E}^{(L)}$ with the magnitude of the charge-exchange term V_1. The proton wave function was calculated for each value of the proton well depths as a function of V_1. Neutron binding energy was held fixed for these calculations.

^{138}Ba$(p,p)^{138}$Ba

The IAR in ^{139}La have been extensively studied using the ^{138}Ba$(p,p)^{138}$Ba reaction.[41] Systematic studies of the IAR in the various Lanthanum isotopes have been reported by Williams *et al.*[45] The IAR in ^{139}La have been analyzed by Harney[21] and by

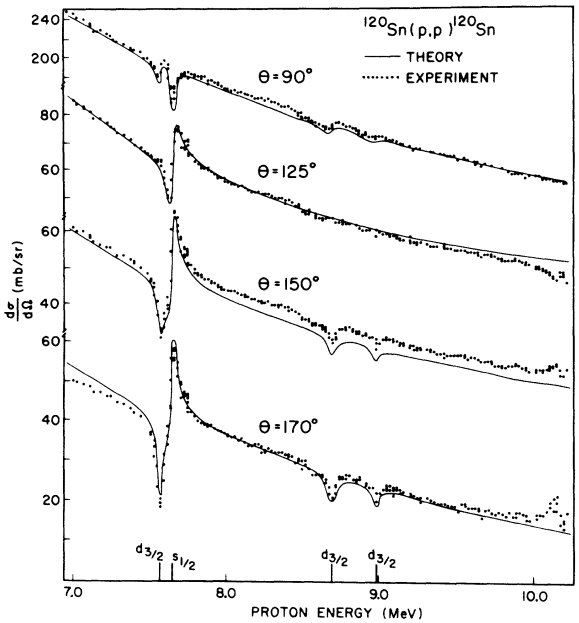

FIG. 8. Comparison of the calculated cross sections with the experimental data for ^{120}Sn$(p,p)^{120}$Sn. The parameters used in the calculation are given in Tables I and V.

TABLE V. Resonance parameters, calculated partial widths, and spectroscopic factors for ^{120}Sn$(p,p)^{120}$Sn. Spectroscopic factors obtained from (d,p) studies are also shown for comparison.

$E_R^{(c.m.)}$ (MeV)	E_{ex} (MeV)	l	j	$\Gamma_{lj}^{(EXP)}$ (keV)	$\Gamma_{lj}^{(L)}$ (keV)	Γ_T (keV)	$(1+Y)^2$	S_{pp}	S_{dp} (Ref. 49)
7.506	0.000	2	$\frac{3}{2}$	7.2	17.92	45	1.11	0.45	0.43
7.585	0.079	0	$\frac{1}{2}$	15.8	54.49	45	1.27	0.37	0.39
8.626	1.120	2	$\frac{3}{2}$	6.5	39.77	78	1.23	0.20	0.065
8.914	1.408	2	$\frac{3}{2}$	3.1	46.63	55	1.27	0.09	0.029

Bund.[14] The data of Ref. 41 and the calculated cross sections are displayed in Fig. 5. The extracted resonance parameters and the spectroscopic factors are given in Table IV. The neutron spectroscopic factors of the low-lying states in ^{139}Ba have been reported by Wiedner *et al.*[46] and von Ehrenstein *et al.*[47] In Table IV the results obtained by Ehrenstein *et al.*,[47] using a zero-range potential with a radial cutoff, are shown for comparison. Though there is possibly some ambiguity due to the numerous overlapping resonances in the region from 11–12 MeV, we found that by far the best fits were obtained by assigning values of +0.5, −0.2, and −0.2 to the resonance mixing phases of the $f_{5/2}$ (11.633), $f_{5/2}$ (11.826), and $p_{1/2}$ (12.092) resonances, respectively. Other than the $f_{7/2}$ resonance, for which we find a much higher spectroscopic factor, our results agree well with those of the (d,p) work. In Figs. 6 and 7 the dependence of the Lane widths $\Gamma_{\lambda E}^{(L)}$ upon the radius parameter r_0 and the magnitude of the charge-exchange term V_1 is displayed.

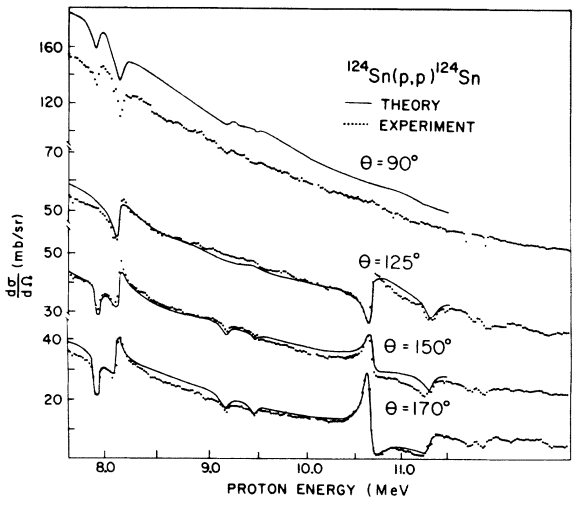

FIG. 9. Comparison of the calculated cross sections with the experimental data for ^{124}Sn$(p,p)^{124}$Sn. The parameters used in the calculation are given in Tables I and VI.

^{120}Sn$(p,p)^{120}$Sn

Figure 8 shows the elastic scattering data on ^{120}Sn taken at the University of Texas. The parameters of the four resonances observed from 7–9 MeV are given in Table V. The $2d_{3/2}$ and $3s_{1/2}$ are separated by only 79 keV, making the fitting somewhat more difficult. The two $l=2$ resonances were assigned a j value of $\frac{5}{2}$ by Richard *et al.*,[48] but the analysis presented here assumes a j value of $\frac{3}{2}$ for each. The spectroscopic factors for the first and second resonances agree very well with those given in Ref. 48, though the last two do not. We were unable to find any combination of parameters for the closely spaced $d_{3/2}$ and $s_{1/2}$ resonances which would give a good fit if the resonance mixing phase is zero. However, by choosing $\phi_\lambda = 0.4$ we were able to obtain a very good fit. As an illustration of the effect, consider the 125° data, where the $l=2$ resonance gives almost no contribution. With a zero phase and the same resonance parameters, the theoretical curve would reach a minimum at about 43 mb/sr and a maximum at about 67 mb/sr; i.e., considerably below the experimental curve at both places. One could perhaps fit the maximum by considerably increasing the partial width, but then the minimum would be even lower than before. Application of the positive phase, however, shifts both portions of the curve upwards to fit the data well.

^{124}Sn$(p,p)^{124}$Sn

The data for ^{124}Sn were taken at the University of Texas over an energy range from 7.6–11.9 MeV and are shown in Fig. 9. There are six resonances present and their parameters are given in Table VI. The potentials used are given in Table I. Note that the well depth that was obtained is fairly small and, as in the other cases, contains an energy dependence. The spectroscopic factors obtained compare well with those of Schneid, Prakash, and Cohen,[49] also given in Table VI. Since the 90° data is not fitted in magnitude, the experiment was run again, and the values given were confirmed. Using different potential parameters

TABLE VI. Resonance parameters, calculated partial widths, and spectroscopic factors for ^{124}Sn$(p, p_0)^{124}$Sn. Spectroscopic factors obtained from (d, p) studies are also included for comparison.

$E_R^{(c.m.)}$ (MeV)	E_{ex} (MeV)	l	j	$\Gamma_{lj}^{(EXP)}$ (keV)	$\Gamma_{lj}^{(L)}$ (keV)	Γ_T (keV)	$(1+Y)^2$	S_{pp}	S_{dp} (Ref. 49)
7.880	0.000	2	$\frac{3}{2}$	6.2	19.9	45	1.14	0.35	0.34
8.065	0.185	0	$\frac{1}{2}$	11.3	65.3	50	1.32	0.23	0.25
9.104	1.224	(2)	$(\frac{3}{2})$	2.7	46.1	78	1.28	0.13	0.039
9.386	1.505	(2)	$(\frac{3}{2})$	1.5	52.4	55	1.32	0.06	0.023
10.585	2.705	(3)	$(\frac{7}{2})$	21.5	45.0	85	1.40	0.67	···
11.200	3.320	(1)	$(\frac{3}{2})$	23.4	106.9	120	2.36	0.51	0.340

was also to no avail, so the discrepancy is not understood. The resonances in ^{124}Sn were fit with the resonance mixing phases equal to zero for all the resonances.

VI. DISCUSSION

The present method for obtaining spectroscopic factors from IAR observed in elastic scattering of protons is based upon the shell-model theory of IAR. It employs the phenomenological optical potential only to parametrize the background part of the energy-averaged scattering matrix elements predicted by the shell-model theory. The *form* of the energy-averaged S matrix elements employed in the analysis agrees with that predicted by most resonance theories. Thus, the parameters extracted by us may also be interpreted readily within other frameworks. We find that the dependence of the calculated width $\Gamma_{\lambda E}^{(L)}$ (and hence the spectroscopic factor) on the potential parameters is small. The optical-model parameters, on the other hand, are to be subjected to the constraints discussed in Secs. II and III; consequently the calculated widths are well determined. The damping of the wave functions inside the nucleus arising from the nonlocality of the optical potential is found to have a significant effect on the results. Indeed, if the nonlocality correction were not made, all the spectroscopic factors arrived at in this analysis would decrease by about 30%. We believe that this damping is a real effect and cannot be ignored in this analysis, since the nuclear interior makes a large contribution in the expression (2.20) for the partial width. The nonlocality length was, however, held fixed at the value $\alpha = 0.85$ F throughout the analysis. Experimental data on the IAR considered in this paper are consistent in general with the assumption of zero resonance mixing phase. In some cases, however, the best fit is obtained with a slightly positive resonance mixing phase. This is particularly true of the $s_{1/2}$ resonance in ^{121}Sb. A nonzero value of the resonance mixing phase tends to shift the entire resonance up or down depending upon the scattering angle and l value of the resonance. We believe that positive values of the resonance mixing phase, of the same order as given in Table II, correspond to the actual situation.

In general, the resonance mixing phase is due to the correlation between the matrix elements $V^{(\Sigma i)}$ connecting the analog state with the complicated background states and the matrix element $V_{\mu\epsilon}^{(i)}$ connecting the background states Φ_i with the open proton channel λ. The evaluation of the resonance mixing phase based upon Eqs. (2.15) and (2.17) assumes that the above-mentioned correlation is essentially due to the indirect coupling between the analog state and the complicated states via the open proton channels. This contribution to the resonance mixing phase arises from what is termed external mixing by Robson[2] and Mekjian and MacDonald.[11] Contributions arising from internal mixing have not been considered in the present framework. The small values of the resonance mixing phase indicate that in heavy nuclei the above-mentioned correlation is insignificant.

ACKNOWLEDGMENTS

The authors acknowledge helpful discussions with H. A. Weidenmüller during several stages of this work. This work has also profited from numerous discussions with W. R. Coker, K. P. Lieb, C. F. Moore, P. Richard, and T. Tamura.

*Work supported in part by the U. S. Atomic Energy Commission.

[1]J. D. Fox, C. F. Moore, and D. Robson, Phys. Rev. Letters 12, 198 (1964).

[2]D. Robson, Phys. Rev. 137, B535 (1965).

[3]E. P. Wigner and L. Eisenbud, Phys. Rev. 72, 29 (1947).

[4]A. M. Lane and R. G. Thomas, Rev. Mod. Phys. 30, 257 (1958).
[5]C. Mahaux and H. A. Weidenmüller, Nucl. Phys. A94, 1 (1967).
[6]H. A. Weidenmüller, Nucl. Phys. A99, 269, 289 (1967).
[7]C. Mahaux and H. A. Weidenmüller, *Shell-Model Approach to Nuclear Reactions* (John Wiley & Sons, New York, 1969).
[8]A. F. R. De Toledo Piza and A. K. Kerman, Ann. Phys. (N.Y.) 43, 363 (1967).
[9]A. K. Kerman and A. F. R. De Toledo Piza, Ann. Phys. (N.Y.) 48, 173 (1968).
[10]R. O. Stephen, Nucl. Phys. A94, 192 (1967).
[11]A. Mekjian and W. M. MacDonald, Nucl. Phys. A121, 385 (1968).
[12]T. Tamura, Phys. Rev. 185, 1256 (1969).
[13]S. A. A. Zaidi and P. Dyer, Phys. Rev. 185, 1332 (1969).
[14]G. W. Bund, Ph.D. thesis, University of Washington, 1968 (unpublished); G. W. Bund and J. S. Blair, Nucl. Phys. A144, 384 (1970).
[15]H. Bledsoe, Ph.D. thesis, University of Texas, 1970 (unpublished); H. Bledsoe and T. Tamura, Nucl. Phys. A164, 191 (1971).
[16]H. L. Harney and H. A. Weidenmüller, Nucl. Phys. A139, 241 (1969).
[17]W. M. MacDonald, in *Isobaric Spin in Nuclear Physics*, edited by J. D. Fox and D. Robson (Academic Press Inc., New York, 1966).
[18]L. I. Garside and W. M. MacDonald, Phys. Rev. 138, B582 (1965).
[19]D. Robson and A. M. Lane, Phys. Rev. 161, 982 (1967).
[20]N. Auerbach, J. Hüfner, A. K. Kerman, and C. F. Shakin, in *Nuclear Isospin*, edited by J. D. Anderson, S. D. Bloom, J. Cerny, and W. W. True (Academic Press Inc., New York, 1969).
[21]H. L. Harney, Nucl. Phys. A119, 591 (1968).
[22]H. A. Weidenmüller and K. Dietrich, Nucl. Phys. 83, 332 (1966).
[23]A. M. Lane, Nucl. Phys. 35, 676 (1962).
[24]C. Mahaux and H. A. Weidenmüller, Nucl. Phys. 89, 33 (1966).
[25]R. Lipperheide, Nucl. Phys. A105, 545 (1967).
[26]J. P. Bondorf, S. Jägare, and H. Lütken, Phys. Letters 21, 185 (1966); in *Isobaric Spin in Nuclear Physics* (see Ref. 17).
[27]T. Tamura, Phys. Letters 22, 644 (1966); in *Isobaric Spin in Nuclear Physics* (see Ref. 17).
[28]E. H. Auerbach, C. B. Dover, A. K. Kerman, R. H. Lemmer, and E. H. Schwarcz, Phys. Rev. Letters 17, 1184 (1966); in *Isobaric Spin in Nuclear Physics* (see Ref. 17).
[29]S. A. A. Zaidi and S. Darmodjo, Phys. Rev. Letters 19, 1446 (1967).
[30]S. A. A. Zaidi and W. R. Coker, Phys. Rev. C 4, 236 (1971).
[31]H. Bledsoe and T. Tamura, to be published.
[32]R. G. Clarkson, P. von Brentano, and H. L. Harney, Nucl. Phys. A161, 49 (1971).
[33]R. G. Clarkson, P. von Brentano, and M. Dost, Phys. Rev. Letters 26, 656 (1971).
[34]A. K. Kerman, in *Nuclear Isospin* (see Ref. 20).
[35]F. G. Perey and B. Buck, Nucl. Phys. 32, 353 (1962).
[36]A. D. MacKeller, J. F. Reading, and A. K. Kerman, Phys. Rev. C 3, 460 (1971).
[37]M. Coz, A. D. MacKeller, and L. G. Arnold, Ann. Phys. (N.Y.) 58, 504 (1970); M. Coz, L. G. Arnold, and A. D. MacKeller, *ibid.* 59, 219 (1970).
[38]H. Fiedeldey, Nucl. Phys. 77, 149 (1967); A96, 463 (1967).
[39]F. G. Perey, Phys. Rev. 131, 745 (1963).
[40]S. A. A. Zaidi, J. L. Parish, J. G. Kulleck, C. F. Moore, and P. von Brentano, Phys. Rev. 165, 1312 (1968).
[41]H. Seitz, D. Rieck, P. von Brentano, J. P. Wurm, and S. A. A. Zaidi, Nucl. Phys. A140, 673 (1970), and references therein.
[42]S. Darmodjo, Ph.D. thesis, University of Texas, 1968 (unpublished).
[43]A. F. Jeans, W. Darcey, W. G. Davies, K. N. Jones, and P. K. Smith, Nucl. Phys. A128, 224 (1969).
[44]G. J. Igo, P. D. Barnes, E. R. Flynn, and D. D. Armstrong, Phys. Rev. 177, 1831 (1969).
[45]N. Williams, G. C. Morrison, J. A. Nolen, Jr., Z. Vager, and D. von Ehrenstein, Phys. Rev. C 2, 1539 (1970).
[46]C. A. Wiedner, A. Hensler, J. Solf, and J. P. Wurm, Nucl. Phys. A103, 433 (1967).
[47]D. von Ehrenstein, G. C. Morrison, J. A. Nolen, and N. Williams, Phys. Rev. C 1, 2066 (1970).
[48]P. Richard, C. F. Moore, J. A. Becker, and J. D. Fox, Phys. Rev. 145, 971 (1966).
[49]E. J. Schneid, A. Prakash, and B. L. Cohen, Phys. Rev. 156, 1316 (1966).